Critical velocities in ^{3}He-^{4}He mixtures below 100 mK

J. C. H. Zeegers, R. G. K. M. Aarts, A. T. A. M. de Waele, and H. M. Gijsman
Eindhoven University of Technology, P. O. Box 513, 5600 MB Eindhoven, The Netherlands
(Received 23 April 1991; revised manuscript received 18 September 1991)

Hydrodynamic properties of dilute mixtures of ^{3}He and ^{4}He were investigated below 100 mK by measuring the thermodynamic properties of the solution in various flow impedances as functions of the ^{3}He velocity. The ^{4}He component in the impedances was practically always macroscopically at rest. If the flow impedances consisted of a bundle of metal or glass capillaries, a distinct critical velocity was observed above which the ^{4}He chemical-potential difference across the impedance was nonzero. The critical velocity of capillaries with diameter d roughly follows a $\ln(d)/d$ dependence. In the critical-velocity region, the amplitude of the pressure fluctuations was observed to be relatively large and strongly velocity dependent. The characteristic time for transient effects in the flow system changed abruptly at the critical velocity. There are indications for the existence of a second critical velocity. In flow impedances with an annular cross section, no critical velocities were observed.

I. INTRODUCTION

In this paper the results are described of an experimental investigation of the hydrodynamics of ^{3}He–^{4}He mixtures below 100 mK. The theoretical basis for the hydrodynamics of ^{3}He–^{4}He II mixtures was formulated by Khalatnikov in 1965.[1] He treated the superfluid ^{4}He component in many aspects as the equivalent of a vacuum in which the ^{3}He quasiparticles are moving as a viscous gas (the mechanical-vacuum model). Wheatley, Rapp, and Johnson[2] measured the viscous heating in ^{3}He flowing through ^{4}He II at low velocities and found agreement with this model. However, later on it was found that for high ^{3}He velocities the ^{3}He flow is strongly impeded by the ^{4}He II component. This dissipative effect is called mutual friction. Castelijns *et al.*[3] gave a phenomenological description of the mutual friction in capillaries for high velocities (the mutual-friction model).

In 1985 there were thus two different models describing the flow properties of ^{3}He moving through superfluid ^{4}He: for low ^{3}He velocities the mechanical-vacuum model and for high velocities the mutual-friction model. The behavior in the intermediate velocity range was unknown. From the analogy with the flow properties of pure ^{4}He II interesting flow phenomena were expected to occur. In this paper we describe the results of the investigations in this intermediate regime.

The experiments were performed in a ^{3}He circulating dilution refrigerator, which is the natural instrument for studying the hydrodynamics of ^{3}He–^{4}He II mixtures at low temperatures. Measurements of the temperature, ^{3}He molar fraction, and pressure differences across the flow channels as functions of the ^{3}He flow rate were carried out in roughly the same setup as used previously by Castelijns *et al.*[3] As the ^{3}He circulation rate of this machine was fairly large, usually a large number of capillaries had to be placed in parallel (≈ 100) in order to reach the intermediate velocity region.

In this paper we will give the main expressions of the mechanical-vacuum model, the mutual-friction model, and the Vinen model.[4] Next we describe the experimental setup and measuring techniques. During this investigation the flow properties of many different flow impedances were determined. In this paper we have to limit the presentation of the experimental results to some typical examples of the flow dependencies of the temperature, ^{3}He molar fraction, pressure, and ^{4}He chemical-potential differences across a small number of flow channels.

For circular capillaries there proved to be a well-defined value of the velocity where mutual friction sets in. This is called the (first) critical velocity. In some cases there was also a kink in the velocity dependence of the downstream parameters. This is an indication for the existence of a second critical velocity.

Time-dependent effects in the critical velocity region will be described. The pressure fluctuations were analyzed using fast Fourier transform (FFT). At velocities in the region of first critical velocity the amplitude of the pressure fluctuations was strongly velocity dependent. The same feature was observed at velocities around the second critical velocity. Preliminary results were presented earlier.[5,6] As part of this investigation also the viscosity of saturated ^{3}He-^{4}He solutions was measured.[7]

The existence of critical velocities is a general phenomenon in pure ^{4}He II and in ^{3}He-^{4}He mixtures. At Leiden University, Mudde and van Beelen[8] performed counterflow experiments in ^{3}He–^{4}He II mixtures in the 1.3–1.7-K range. In Japan, the flow properties were examined of a system in which ^{4}He was forced to flow through a capillary at temperatures around 0.7 K.[9] In experiments at temperatures above 0.7 K, the ^{4}He excitations (normal component) play an important role in the flow properties. The experiments described here are confined to the temperature range below 200 mK where the effects of the normal component of the ^{4}He II can be neglected. This greatly simplifies the experiments and the analysis of the results.

II. MODELS

A. Introduction

The hydrodynamics of superfluid ^{4}He is reviewed by Tough[10] and Donnelly and Swanson.[11] The thermodynamic and hydrodynamic properties of mixtures were reviewed by de Waele and Kuerten.[12] In this section we will only give a short outline of the basic principles and assumptions.

We assume that there is only an axial velocity component and that the ^{3}He mole fraction x, the temperature T, and the pressure p only depend on the axial parameter z. We will consider macroscopically stationary flow states in which the ^{4}He velocity is zero, so the relative velocity of the two components is equal to the ^{3}He velocity v.

The flow impedances in this work were either (bundles of) capillaries with a circular cross section, or annular channels with a ring-shaped cross section. In both cases the length is denoted by l. The cross-sectional area of one channel is A. The circular capillaries have diameter d. The annular channels have spacing w and diameter D, with $w \ll D$. The pressure gradient in the case of laminar flow is given by

$$dp/dz = -\eta \zeta \dot{n} V_3 , \tag{1}$$

where η is the viscosity, ζ is a geometry-dependent impedance factor, $\dot{n}$ the molar ^{3}He flow rate, and V_3 the volume of the solution containing 1 mol of ^{3}He. For V_3 we will assume the constant value of 415 cm^3/mol, which is justified for ^{3}He mole fractions near $x_0 = 0.066$, the concentration of the saturated solution at 0 K. For capillaries $\zeta = 128/(\pi d^4)$; for annular channels $\zeta = 12/(\pi D w^3)$. The parameter N will represent the number of capillaries or annular flow channels which together form the flow impedance under investigation.

In a macroscopically steady state the gradient of the molar ^{4}He chemical potential (μ_4) and the mutual friction force density $\mathbf{F}_{sn}$ (exerted by the normal component on the superfluid component) are related according to the equation

$$\nabla \mu_4 = V_4^0 \frac{\rho}{\rho_s} \mathbf{F}_{sn} , \tag{2}$$

where V_4^0 is the molar ^{4}He volume , ρ the density of the solution, and ρ_s is the superfluid density.

B. Low-temperature approximations

At low temperatures ($T < 0.5$ K) the influence of ^{4}He excitations on the flow properties is negligible, so in our case the normal component can be considered to consist of the ^{3}He quasiparticles only. The normal component density ρ_n satisfies the relation $\rho_n = \rho - \rho_s$. With $\rho_n = \rho_3 m^*/m_3$, where ρ_3 is the ^{3}He density and $m^*/m_3 = 2.46$ is the ratio of the ^{3}He quasiparticle effective mass and the ^{3}He atomic mass,[13] one finds $\rho_n = 17.71$ kg/m^3 at low temperatures and for a 6.6% mixture. Furthermore, in our analysis we used $V_4^0 = 27.58$ cm^3/mol and $\rho = 140$ kg/m^3.

In our experiments the flow is adiabatic. In that case the osmotic enthalpy H_3^{os} is constant.[14] At zero pressure, in the low-temperature limit and for $x \simeq x_0$ the osmotic enthalpy can be approximated by the relation[13]

$$H_3^{os} \simeq H_x (x - x_0) + H_T T^2 , \tag{3}$$

where $H_x = 17.58$ J/mol and $H_T = 84.06$ J/mol K^2.

In this paper T, x, p, and μ_4 at the entrance of a flow channel are indicated with a lower index m, for "mixing chamber." The downstream quantities (in the experimental space) get the lower index e. In the case of adiabatic flow H_3^{os} is constant and Eq. (3) gives

$$T_e^2 = T_m^2 + a(x_m - x_e) , \tag{4}$$

with $a = H_x/H_T$. In the low-temperature limit, the specific heat of the solution containing 1 mol of ^{3}He is given by $C_3 \simeq C_0 T$ with $C_0 = 104.3$ J/mol K^2. The ^{3}He viscosity η is approximated by

$$\eta \simeq \eta_0 / T^2 , \tag{5}$$

where we took $\eta_0 = 5 \times 10^{-8}$ s Pa K^2 as a good approximation in our temperature range.[7]

C. The mechanical-vacuum model

In this model the ^{3}He quasiparticles and the superfluid component move without mutual friction, $\mathbf{F}_{sn} = 0$. The ^{4}He is in the laminar flow state, so in the steady state μ_4 is constant [Eq. (2)]

$$\mu_{4e} = \mu_{4m} . \tag{6}$$

The temperature T_e is given by

$$T_e = T_m (1 + \nu)^{1/4} . \tag{7}$$

For ease of notation we introduced a flow-rate and temperature-dependent parameter ν as

$$\nu = 4 \frac{\zeta l V_3^2 \eta_0}{N C_0 T_m^4} \dot{n} . \tag{8}$$

The downstream pressure p_e satisfies

$$p_e = p_m - (C_0/2V_3) T_m^2 (\sqrt{1+\nu} - 1) . \tag{9}$$

The ^{3}He molar fraction x_e in the experimental space results from Eqs. (4) and (7)

$$x_e = x_m - (T_m^2/a)(\sqrt{1+\nu} - 1) . \tag{10}$$

D. The mutual-friction model

For the mutual-friction model, i.e., for high ^{3}He velocities, Castelijns found the following empirical relations:

$$\mu_{4e} = \mu_{4m} + \chi l j^3 , \tag{11}$$

$$T_e^2 = T_m^2 + a \gamma'' l j^3 , \tag{12}$$

$$p_m \approx p_e , \tag{13}$$

$$x_e = x_m - \gamma'' l j^3 , \tag{14}$$

where $\gamma''=14\times10^{-9}$ $s^3 m^5/mol^3$, $\chi=11\times10^{-9}$ $kg\,s\,m^7/mol^4$. The molar ^{3}He flux $j=\dot{n}/NA$ is also given in terms of the ^{3}He velocity v by

$$j=v/V_3 \ . \tag{15}$$

E. The Vinen model

Hall and Vinen[15] and Vinen[4] proposed a model for the growth and decay of a vortex tangle as a function of time. The equation describing the evolution of the average vortex line length density L reads

$$\dot{L}=\tfrac{1}{2}B\chi_1\frac{\rho_n}{\rho}v\frac{A-A'}{A}L^{3/2}-\frac{\kappa}{2\pi}\chi_2L^2 \ . \tag{16}$$

Here $\kappa=h/m_4$ is the quantum of circulation, with h Planck's constant, and m_4 the mass of a helium-4 atom; χ_1, χ_2, and B are constants of order unity. The parameter A' represents the cross-sectional area of a layer near the wall of thickness $\frac{1}{2}\delta/\sqrt{L}$ with δ a constant of order unity. For circular channels

$$\frac{A-A'}{A}=\left[1-\frac{\delta}{d\sqrt{L}}\right]^2 , \tag{17}$$

and for annular channels

$$\frac{A-A'}{A}=1-\frac{\delta}{w\sqrt{L}} \ . \tag{18}$$

In the stationary state $\dot{L}=0$. Apart from $L=0$ the solution of Eq. (16) is

$$\pi B\chi_1\frac{\rho_n}{\rho}v\frac{A-A'}{A}-\chi_2\kappa\sqrt{L}=0 \ . \tag{19}$$

In terms of the Vinen model, the mutual-friction force density is written as

$$F_{sn}=\tfrac{1}{3}B\frac{\rho_s\rho_n\kappa}{\rho}vL \ . \tag{20}$$

Combination of Eqs. (2) and (20) gives

$$\Delta\mu_4=\tfrac{1}{3}BV_4^0\rho_n lvL \ . \tag{21}$$

For later use we define the parameters Γ, α, and m as follows:

$$\Gamma=\sqrt{\Delta\mu_4/lv} \ , \tag{22}$$

$$\alpha=\frac{\chi_2}{\pi\chi_1}\left[\frac{3\kappa\rho^2}{B^3\rho_n^3V_4^0}\right]^{1/2} , \tag{23}$$

$$m=\delta\sqrt{\tfrac{1}{3}BV_4^0\rho_n\kappa} \ . \tag{24}$$

The parameter Γ can be derived directly from the measurements. The parameters α and m contain the unknown liquid parameters (δ, B, χ_1, and χ_2) and will be derived from a best fit to the measured Γ-vd dependencies. For circular capillaries Eq. (19) yields the product

$$vd=\alpha\frac{(\Gamma d)^3}{(\Gamma d-m)^2} \ ; \tag{25}$$

and, for annular flow channels, the product

$$vw=\alpha\frac{(\Gamma w)^2}{\Gamma w-m} \ . \tag{26}$$

The (vd)-(Γd) and the (vw)-(Γw) curves have the same shape. When $\Gamma d\gg m$ or $\Gamma w\gg m$, which holds for high flow rates or large cross sections, Eqs. (25) and (26) both reduce to

$$v\simeq\alpha\Gamma \ . \tag{27}$$

III. EXPERIMENTAL SETUP AND MEASURING TECHNIQUES

A. The low-temperature part of the system

The experiments were carried out in a dilution refrigerator[3] which was suspended from a 6-ton concrete block mounted on air springs for vibration isolation. The main experimental arrangement is presented in Fig. 1. In this system the mixing chamber had a long tail. Thus the flow properties of 38-cm long channels, mounted inside the mixing chamber, could be investigated. The mixing chamber temperature T_m was adjusted with a heater attached to the tube connecting the concentrated side of

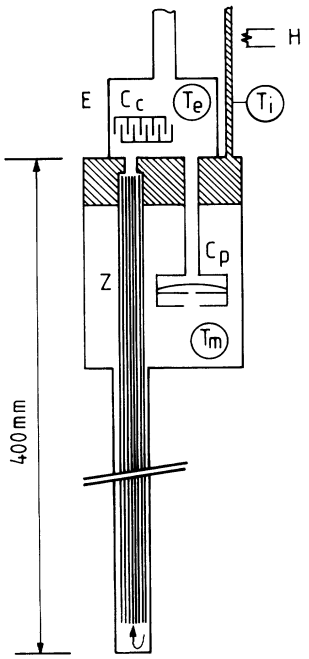

FIG. 1. Schematic drawing of the low-temperature part of the flow system; Z represents the flow impedance, which in this case is mounted inside the mixing chamber; E is the experimental space where the downstream properties are measured; C_c represents the capacitor measuring the concentration; C_p the pressure cell; T_i, T_m, and T_e represent Speer resistance thermometers. The shaded area represents the concentrated phase. The ^{3}He entering the mixing chamber can be heated by a heater H.

the heat exchangers and the mixing chamber. The measurements of the pressure difference Δp, the downstream temperature T_e, and ^{3}He molar fraction x_e as functions of the ^{3}He flow rate $\dot{n}$ were carried out at constant T_m.

In a system slightly different from the one presented in Fig. 1, the flow channel was mounted outside the mixing chamber so there was practically no limit to the length of the impedances. The flow properties of coiled tubes with an inner diameter up to 0.74 cm and length 6 m were investigated in this setup.

In addition to the devices mentioned above, the mixing chamber and experimental space could be equipped with additional pressure cells, thermometers, shunting tubes and superleaks, vibrating wire viscometers, capacitors for concentration measurement, etc. The determination of the flow characteristics of a particular flow impedance usually took one week. The refrigerator had to be warmed up to room temperature and opened for replacing the impedance. During this investigation, this was repeated about 140 times.

B. Determination of the thermodynamic parameters

At several points in the system the temperature was measured with 220-Ω Speer carbon resistance thermometers[16,17] which were calibrated with a cerium magnesium nitrate thermometer[16] (CMN) in combination with two superconducting fixed-point devices.[18,19] The calibration was carried out with the fixed-point devices and the CMN thermometer in the dilute phase of the mixing chamber at the same time. In the 20–200 mK range the calibration has an accuracy of about 0.2 mK. Below 15 mK a CMN thermometer was used.

The measurement of the ^{3}He molar fraction x_e was based on the concentration dependence of the dielectric constant of mixtures[20] using a parallel plate air capacitor C_c. The capacitor was calibrated in two different ways: with the temperature dependence of C_c in the saturated solution (^{3}He concentration x_s) using the dx_s/dT^2 value determined by Abraham *et al.*,[21] and from the capacitance change when all ^{3}He was removed from the dilution refrigerator system ($x=0$). For a capacitor with nominal value of 34 pF the two calibrations yielded $dC_c/dx=-55.3$ aF and were consistent within 1.5 aF. The following calibration was obtained:

$$\frac{1}{C_c}\frac{dC_c}{dx}=-0.0163 \ . \tag{28}$$

In one setup the accuracy of the above calibration was estimated to be 3%; in another it was 1%. Concentration variations of about 20 or 10 ppm could be detected. We observed long-term drifts (day-to-day changes) of the capacitance corresponding to concentration differences on the order of 100 ppm which are not well understood.

When a new impedance was installed, the value of C_c at zero flow rate C_{c0} changed slightly due to parasitic capacitances. In order to determine C_{c0}, we extrapolated the C_c-$\dot{n}$ dependence to zero flow rate, using Eq. (10) as a guide. This introduces an error in the absolute value of x of about 300 ppm.

Pressure differences were measured with a capacitive pressure cell[22] calibrated in a ^{4}He cryostat by means of a liquid ^{4}He column. Its capacitance C_p was measured with a bridge in combination with a lock-in amplifier. The zero flow value (C_{p0}) was again obtained from the extrapolation of the C_p-$\dot{n}$ curve to zero $\dot{n}$. The C_{p0} value between different runs varied a few percent. We corrected the calibration for this variation assuming that the change in C_{p0} was caused by a small variation of the distance between the capacitor plates.

For the numerical analysis of the pressure fluctuations (to be discussed later) the off-balance signal from the analog output of the lock-in amplifier was sampled with a sampling time between 3 and 100 ms. The maximum number of points that could be handled was 4096. Frequencies above the Nyquist frequency were avoided by making the time constant of the lock-in amplifier larger than the sampling time.

The chemical potential was calculated from T, x, and p using the low-temperature approximations and the tables from Kuerten *et al.*[13]

The flow rate ($\dot{n}$) was adjusted with the still heater to values between 0.06 and 1 mmol/s. The dependencies of the thermodynamic quantities will be presented as functions of the average ^{3}He velocity v

$$v=\dot{n}V_3/NA \ . \tag{29}$$

The flow rate $\dot{n}$ was measured at the room temperature and contained a small amount of ^{4}He. Only data points where the ^{4}He contribution was less than about 4% were considered.

C. Design of the flow impedances

In the design of the circular flow impedances, we used the property that the $v_c d$ product is approximately constant: $v_c d \approx W \approx 0.10$ cm^2/s. For a given flow impedance, the critical velocity v_c corresponds to a ^{3}He flow rate $\dot{n}_c$. We designed the flow impedances in such a way that the expected $\dot{n}_c$ is about half the maximum flow rate $\dot{n}_m$ (≈ 1 mmol/s) of the dilution refrigerator ($\dot{n}_c \approx \frac{1}{2}\dot{n}_m$). With N circular capillaries in parallel one obtains

$$N=2\dot{n}_m V_3/\pi d W \ . \tag{30}$$

Equation (30) implies, e.g., that about 100 capillaries have to be placed in parallel for $d=0.03$ cm.

The expected temperature jump at v_c can be estimated from Eq. (12). In order to determine v_c accurately, it should be larger than a certain minimum value $\Delta T_{\min}$. This condition can be written as

$$l \geq \frac{2}{a\gamma''}\left[\frac{V_3}{W}\right]^3 T d^3 \Delta T_{\min} \ . \tag{31}$$

E.g., for $T=30$ mK, $\Delta T_{\min}=1$ mK, and $d=0.03$ cm, it follows that $l \geq 4.6$ cm. For tubes with diameters of 1 mm or larger, very long tubes are necessary. Equation (30) and condition (31) set the limitations of the range of capillary diameters available for experimental access.

The diameters of the small-diameter capillaries were

TABLE I. First column: label identifying the flow impedance. The second, third, and fourth columns show the number of tubes, length, and diameter, respectively. The fifth column gives the tube material (CN: cupronickel, St: stainless steel, Gl: glass). The sixth column gives v_c, and the seventh the product $v_c d$, respectively. The last column gives T_m at which the measurements were carried out. The uncertainties in the last digit of the different parameters are indicated by numbers in parentheses.

No.	N	l (cm)	d (cm)	Tube material	v_c (cm/s)	$v_c d$ (cm^2/s)	T_m (mK)
Z_A	70	3.00(1)	0.019(1)	CN	6.5(1)	0.12(2)	27.2/46.0
Z_B	28	2.30(1)	0.0261(5)	CN	7.0(4)	0.183(7)	27.0/36.7/46.0 56.0/65.8/77.0 87.8/97.0/37.0
Z_C	113	19.80(1)	0.030(1)	CN	5.3(1)	0.159(3)	51/75
Z_D	60	17.70(1)	0.030(1)	CN	5.2(4)	0.156(7)	27.2/46
Z_E	19	8.24(1)	0.040(1)	CN	5.0(2)	0.198(6)	46.0
Z_F	34	19.90(5)	0.050(1)	CN	3.3(2)	0.163(6)	27.2/46.0
Z_G	15	32.27(1)	0.065(1)	CN	2.47(7)	0.161(5)	46.0
Z_H	13	38.01(1)	0.081(1)	CN	2.2(1)	0.177(5)	27.2/46.0
Z_I	1	1.045(5)	0.120(5)	CN	?	?	37.1/56.0
Z_J	3	20.98(1)	0.180(2)	CN	1.2(1)	0.21(4)	33.9
Z_K	3	187.6(2)	0.180(2)	CN	1.17(6)	0.21(1)	33.0
Z_L	85	5.92(1)	0.0155(10)	St	10(1)	0.15(1)	36.2/46.0
Z_M	1	597.3(5)	0.436(3)	St	0.63(5)	0.27(2)	38.1
Z_N	1	257.1(4)	0.740(25)	St	0.47(4)	0.35(3)	34.9
Z_O	222	0.56(1)	0.0054(10)	Gl	12(5)	0.06(2)	46.0
Z_P	243	2.50(1)	0.012(1)	Gl	9(2)	0.11(1)	46.0
Z_Q	120	7.97(1)	0.0160(5)	Gl	7.9(5)	0.127(5)	46.0
Z_R	96	7.01(1)	0.022(1)	Gl	5.8(6)	0.127(5)	46.0
Z_S	54	17.84(1)	0.029(1)	Gl	5.0(4)	0.145(8)	27.4/46.0/27.4

determined from a photographic picture using a microscope and a marking gauge. With the small-diameter glass capillaries the variations in d amounted to 10–15 %. For the glass tubes of diameter 0.029 cm, the diameter variations were less than 3%. Table I surveys the circular flow channels used in our experiments. For Z_A and Z_O there is an uncertainty in N of 2 and 5, respectively, due to a possible blocking of individual capillaries. In Table II the annular flow channels are presented. The meaning of the term "apparent critical velocity" v_{ca} will be discussed in the next sections. The diameters of the tubes forming the annular flow channels were made on a precision lathe so the accuracy of the width of the annular space was 1 μm. The tube length was chosen to be as long as possible, provided the viscous heating did not become too large. The maximum length, determined by the space in our dilution refrigerator, was about 35 cm.

IV. THE STEADY STATE

A. Introduction

In total the flow properties of more than 25 different flow channels were investigated. In this paper only a selection of typical results is presented; these will be compared with the mechanical-vacuum model (MV) [Eqs. (6)–(10)] and with the mutual-friction model (MF) [Eqs. (11)–(14)]. For ease of comparison, the results of impedances Z_I, Z_D, Z_S, and Z_U will be treated in the same arrangement in Figs. 2, 7, and 10. Each of these impedances represents a certain class of impedances: Z_I was a single circular metal capillary, typical for the flow properties in the high velocity limit; Z_D was a bundle of metal circular capillaries, showing a distinct critical velocity; Z_S was a bundle of glass circular capillaries, showing the more gradual transition at the critical velocity;

TABLE II. Survey of the annular flow channels. This table has the same structure as Table I (GS: German silver, St: stainless steel, Br: brass, Cu: copper).

No.	N	l (cm)	D (cm)	w (μm)	Material	v_{ca} (cm/s)	$v_{ca} w$ (cm^2/s)	T_m (mK)
Z_T	1	2.00(1)	1.0325	50(1)	GS	5.8(5)	0.029(3)	46.0
Z_U	1	6.00(1)	0.7857	101(1)	GS	3.4(4)	0.034(4)	46.0
Z_V	1	6.00(1)	0.792	100(10)	GS	4.2(1)	0.042(1)	32.2/45.2/46.0
Z_W	1	18.00(1)	0.737	150(10)	St	3.3(7)	0.05(1)	32.2/46.0
Z_X	1	31.05(1)	0.731	210(10)	St	2.2(2)	0.044(4)	46.0
Z_Y	3	30.00(1)	0.7890	100(3)	Br	2.5(5)	0.025(3)	39.7
Z_Z	1	10.00(1)	2.6027	1000(1)	Cu	>0.5	>0.05	33.0

finally, Z_U represents the annular type of flow impedances.

B. Circular capillaries

1. p, T, x dependencies

Most of the measurements were carried out decreasing the flow rate in steps. In the preliminary experiments the transition region was explored varying the flow up and down; only once there was an indication for hysteresis (impedance Z_L). The flow channels Z_C and Z_D are the same apart from the number of capillaries. The critical velocities for the two flow channels coincide within the measuring accuracy (Table I). This proves that the interpretation of the results in terms of the velocity v is justified. In the Figs. 2(a)–2(d), the temperature T_e is plotted as a function of v for the four impedances. For the single metal tube [Fig. 2(a)], mutual friction dominates even at the lowest velocities. According to Fig. 9 the critical velocity for this channel with $d=0.12$ cm is estimated to be about 2 cm/s, which is well below the range of the measurement. The agreement with the mutual-friction model expresses the reproducibility of the results obtained before.[3]

Figure 2(b) shows the result obtained with 60 metal capillaries with $d=0.03$ cm in parallel. The critical velocity at 5.2 cm/s is very distinct. For low velocities there is reasonable agreement with Eq. (7). Above the critical velocity the measured T_e is not in agreement with Eq. (12). The discrepancy increases with increasing velocity in this velocity region.

The value of v_c proved to be not (or only weakly) temperature dependent in the temperature range 10–100 mK. This proves that the critical velocity is not due to classical turbulence in the ^{3}He. The Reynolds number,

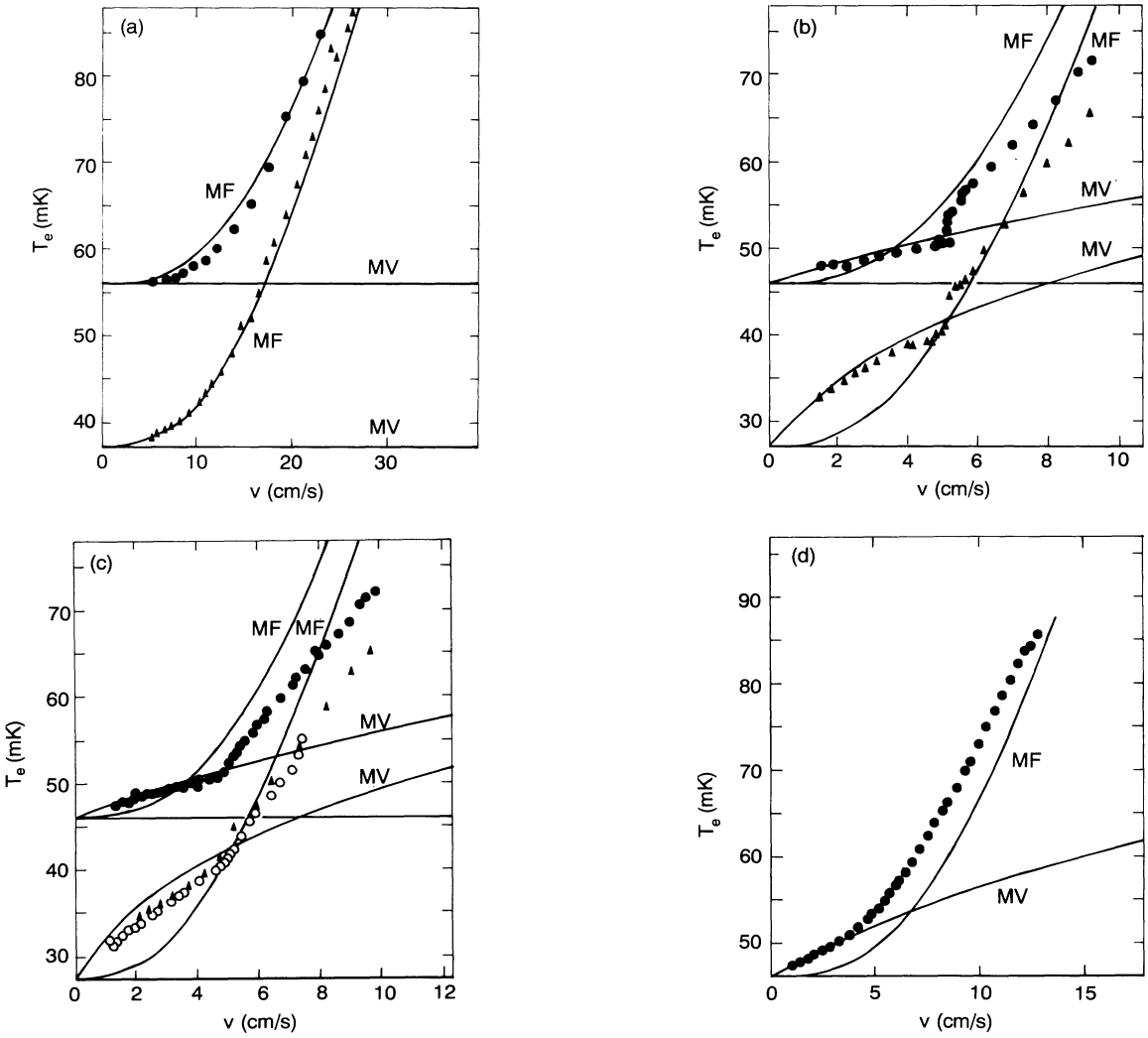

FIG. 2. Downstream temperatures T_e measured as functions of the ^{3}He velocity for different T_m. The values of T_m are represented by horizontal lines. MV and MF represent the temperature T_e calculated with Eqs. (7) and (12), respectively. (a) impedance Z_I, a single metal capillary; ●, $T_m=56.0$ mK; ▲, $T_m=37.1$ mK; (b) impedance Z_D, 60 metal capillaries in parallel; ●, $T_m=46.0$ mK; ▲, $T_m=27.2$ mK; (c) impedance Z_S, 54 glass capillaries in parallel; ○, $T_m=46.0$ mK; ▲ and ●, $T_m=27.4$ mK; (d) impedance Z_U, annular impedance, $T_m=46.0$ mK.

defined by $N_{Re}=vd\rho_n/\eta$, calculated for $v=v_c$, varies from 8 at low temperatures to 80 at high temperatures. Thus v_c is not determined by viscous instability effects as in ordinary liquids. In addition, N_{Re} is much smaller than the critical value of about 2000 which determines the onset of turbulence in ordinary liquids.

Figure 2(c) represents T_e determined with glass capillaries of dimensions similar to the metal capillaries discussed above [Fig. 2(b)]. For glass the transition at v_c was observed to be more gradual. In addition, at some higher velocity, there seems to be a rather abrupt change in slope indicating a second critical velocity (v_{c2}). The results represented in Fig. 2(d) apply to the annular impedance and will be discussed later.

Figure 3 shows an example of the velocity dependence of the ^{3}He molar fraction [compare Fig. 2(b)]. The general features are the same as in the temperature measurements discussed above. Figure 4 shows the pressure differences over flow channels as functions of v for various T_m. In this particular case the transition at v_c at about 7 cm/s is present, but difficult to see. The lines are calculated using a constant value of the viscosity at the mixing-chamber temperature.[7] Relation (9) is satisfied, even for $v > v_c$.[23]

A possible excess pressure due to a force between ^{4}He vortices and the wall is difficult to deduce from our measurements as η depends strongly on the temperature. In Fig. 4 nearly all curves are concave for velocities above about 7 cm/s. However, the curves for $T_m=77$, 87.8, and 97.0 mK are slightly convex. This may be an indication of the excess pressure.

In some occasions (mainly in the lower-temperature range) a pressure drop is observed at the critical velocity (Fig. 5). This is due to the temperature increase [see Fig. 2(b)] and the resulting decrease in the average viscosity in the tube [Eq. (5)].

The heat exchange between the fluid and the walls, and the heat conduction through the liquid in the flow direction were negligible, so the flow was adiabatic. This is confirmed by the T_e^2-x_e plots presented in Fig. 6 where the points follow the lines of constant H_3^{os}.[3,13]

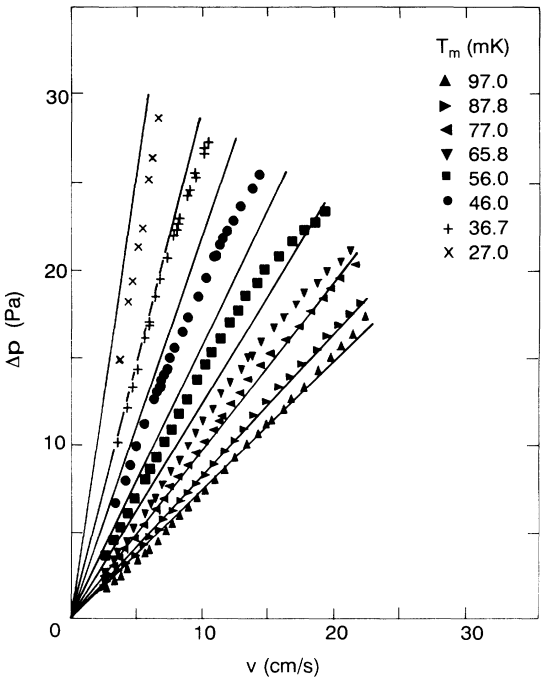

FIG. 4. Pressure differences measured across flow impedance Z_B. The lines are the linear approximations calculated using the measured viscosity (Ref. 7). The mixing-chamber temperatures are given in the inset.

2. The ^{4}He chemical-potential difference

Some typical examples of the ^{4}He chemical-potential difference calculated from the measured p, T, and x, are

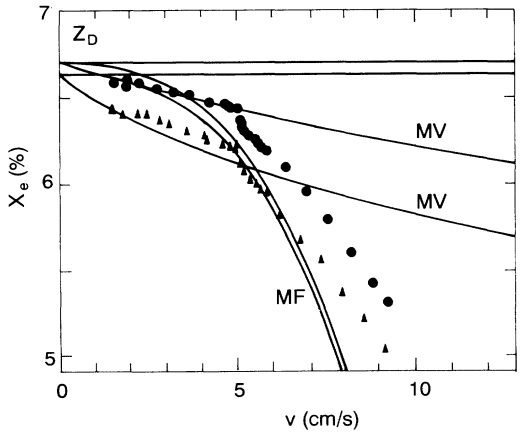

FIG. 3. Typical example of the measured x_e [Z_D, compare Fig. 2(b)] showing a clear critical velocity. The values of x_m are represented by horizontal lines. MV and MF represent the concentration x_e calculated with Eqs. (10) and (14), respectively (●, $T_m=46.0$ mK; ▲, $T_m=27.2$ mK).

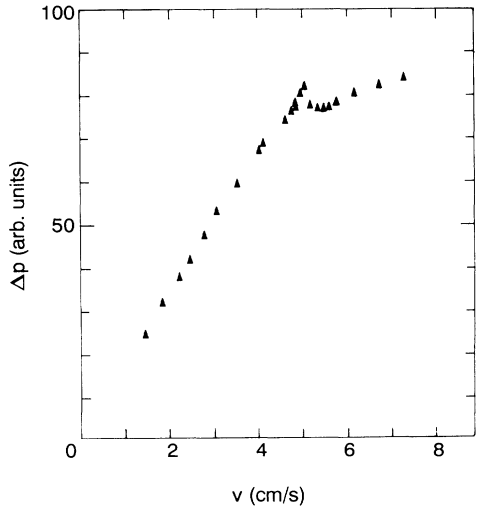

FIG. 5. Example of a (Δp)-v measurement with $T_m=27.2$ mK. In this particular case the peak at the critical velocity is very clear.

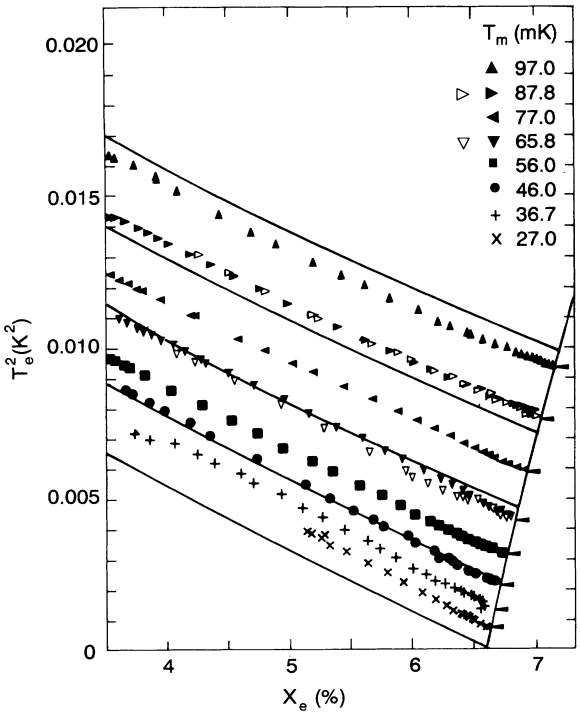

FIG. 6. Typical example of the measured T_e^2-x_e dependencies. Curves of constant enthalpy are also drawn. The line on the right-hand side of the diagrams represents the phase separation line. The arrows indicate T_m^2.

presented in Fig. 7. The results of the impedance Z_I [Fig. 7(a)] are in agreement with Eq. (11) and confirm the mutual-friction model. Figure 7(b) shows $\Delta\mu_4$ for impedance Z_D. The nonzero values of $\Delta\mu_4$ below v_c are caused presumably by the inaccuracy in the determination of the concentration (an uncertainty of 500 ppm leads to an error of about 0.5 mJ/mol). In the analysis we shifted $\Delta\mu_4$ in such a way that $\Delta\mu_4=0$ below the critical velocity. The deviation of the data from the calculated curve shows that Eq. (11) apparently only holds in the high-velocity regime. Figure 7(c) shows the more gradual behavior as found with the glass capillaries. Figure 7(d) will be discussed later.

In some experiments the flow impedance was shunted by a superleak which consisted of a 1.2-cm diameter tube filled with densely packed jeweler's rouge. For the ^{3}He component the flow impedance of the superleak is very high, but the superfluid ^{4}He can flow through it with velocities as large as 20 cm/s without dissipation ($\Delta\mu_4=0$). So with the superleak present the ^{4}He can circulate internally from the mixing chamber through the flow impedance to the experimental space E and back to the mixing chamber via the superleak. Figure 8 gives $\Delta\mu_4$ measured with and without the superleak. For ^{3}He velocities below about 1.2 cm/s the results with and without the superleak both coincide with the mechanical-vacuum model ($\Delta\mu_4=0$). Without the superleak, a nonzero $\Delta\mu_4$ develops at the critical velocity. However, with the superleak $\Delta\mu_4=0$ within experimental accuracy over the entire velocity range.

3. *The $v_c d$ product*

The $v_c d$ product is presented as a function of $\ln(d)$ in Fig. 9. The points roughly follow a straight line corresponding to

$$v_c d = K \ln(d/d_0) , \tag{32}$$

where $K=0.05$ cm^2/s and $d_0=15$ μm. The critical-velocity measurement for one particular type of capillary is quite reproducible. The scatter in the data is perhaps due to the different l/d ratios, the different inlet conditions for the channels, or the difference in the pinning properties of the surface of the flow channels.

4. *Second critical velocity*

In some of the measurements (e.g., in Fig. 8 at 2.5 cm/s) on metal capillaries and in many of the glass capillaries we observed an upward kink in the curves at a velocity which is about twice the critical velocity. This kink is an indication for the existence of a second critical velocity v_{c2} in addition to the (first) critical velocity v_c discussed so far. More evidence for a second critical velocity was obtained from the analysis of the pressure fluctuations to be discussed later.

C. Annular channels

In Fig. 2(d) the T_e-v dependence of an annular flow channel is presented. At low velocities the data coincides fairly well with the mechanical vacuum approximation. There is no well-defined critical velocity as in the metal circular capillaries. In Fig. 7(d) the $\Delta\mu_4$-T dependence is shown. Surprisingly, there is agreement with the high-velocity limit of the mutual-friction model [compare Fig. 7(a)]. This suggests that the critical velocity is well below our detection limit. Furthermore, it shows a geometry-independent mutual friction in the high-velocity limit.

In none of the annular impedances has a critical velocity, defined as a more or less abrupt change in the velocity dependence of the downstream parameters, been observed. The deviation from the mechanical-vacuum model was always gradual [Fig. 2(d)]. The velocity value where the deviations become significant will be called the apparent critical velocity v_{ca}. In order to investigate the values of v_{ca} in more detail we constructed a flow channel with the same cross section as Z_U but five times longer and with three tubes in parallel (Z_Y in Table II). In this case $v_{ca}=2.5$ cm/s, which should be compared with the value of 3.4 cm/s for Z_U. The difference in the values of

TABLE III. Fit of the data with the Vinen model.

No.	α	m [10^{-6} (J s/mol)$^{1/2}$]
Z_I	0.087	
Z_D	0.106	19
Z_S	0.100	23
Z_U	0.084	
Z_B	0.100	23

v_{ca} shows that the value of v_{ca} is mainly determined by the resolution of the measurement. The various v_{ca} values obtained in our experiments are given in Table II.

The behavior of the pressure fluctuations at the "critical" velocity in circular and annular channels is also different, as will be discussed later.

D. Analysis in terms of the Vinen model

We will now discuss the analysis of the data in terms of the Vinen model. The values of m and α were determined by the best fit of Eqs. (25) and (26) to the data. The results of the fitting procedure are presented in Table III and shown as the calculated curves in Figs. 10(a)–10(d). In the cases represented in Fig. 10(b) and 10(c), the parameters α and m could be determined accurately using the presence of a distinct critical velocity and the concave velocity dependence of Γd.

In Fig. 10(a) the measurement with Z_I, the flow impedance consisting of a single tube, is presented. As noted before, the critical velocity could not be measured in this case. The slope of the least-squares straight-line fit based on Eq. (27) yields $\alpha=0.087$. The parameter m could not be determined in this case.

In Fig. 10(d) the measured (Γw)-(vw) dependence of the annular flow impedance is shown. The slope of the straight line [Eq. (27)] yields $\alpha=0.084$, which is practically the same as the value found for flow impedance Z_I, but differs from the value of 0.100 found just above v_c. The constants α and m, derived from the (Γd)-(vd) curves of the circular capillaries [$\alpha=0.1$, $m=20\times10^{-6}$ $(\mathrm{J\,s/mol})^{1/2}$], can be substituted in Eq. (26). The resulting (Γw)-(vw) dependence is also shown in Fig. 10(d) and is not in agreement with the data.

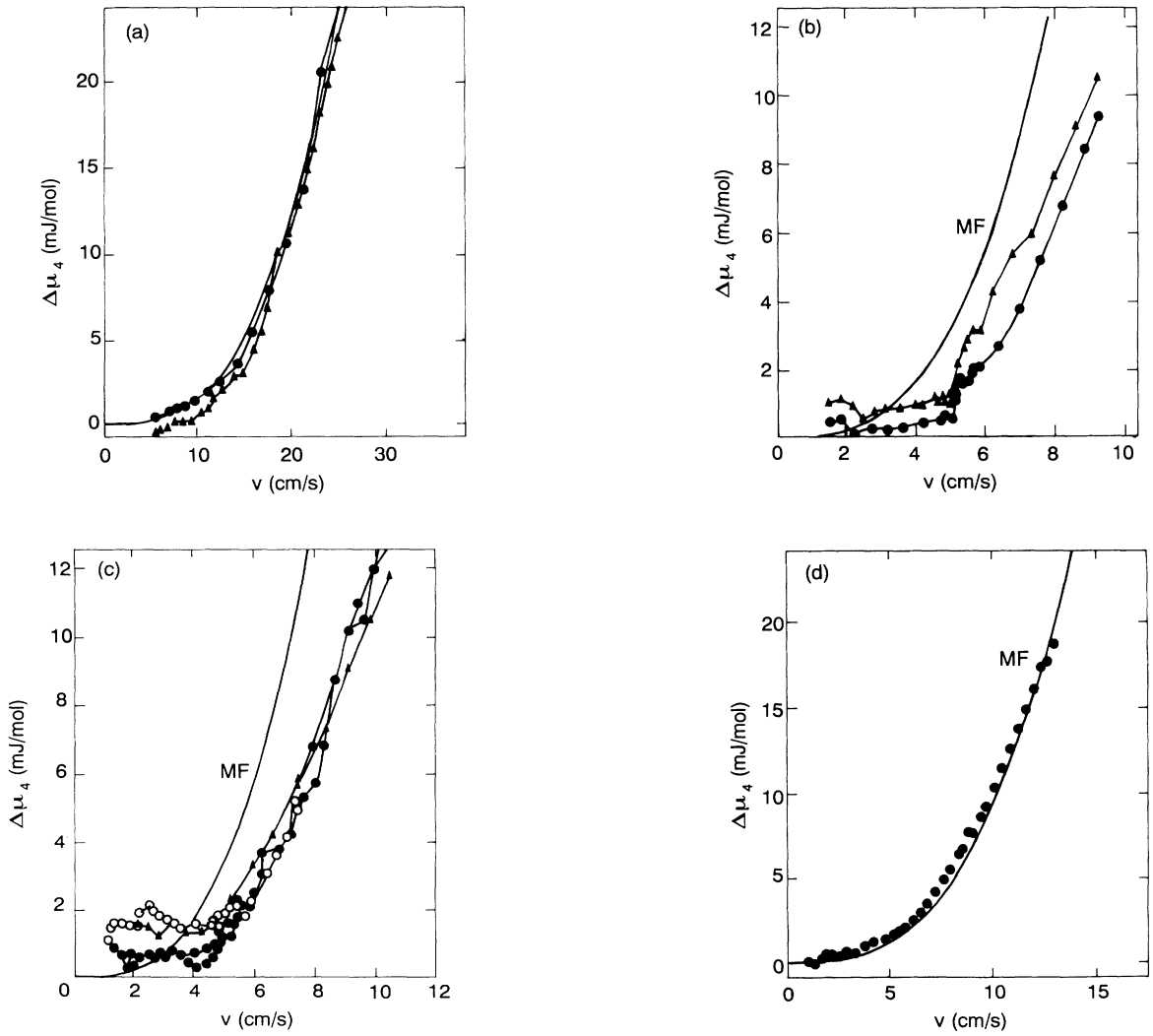

FIG. 7. Examples of the measured $(\Delta\mu_4)$-v dependencies. The lines connecting the points are guides to the eye. Calculated $(\Delta\mu_4)$-v dependencies using Eq. (11) are also shown (MF). The mechanical-vacuum model gives $\Delta\mu_4=0$ in all cases. (a) impedance Z_I; ●, $T_m=56.0$ mK; ▲, $T_m=37.1$ mK; (b) impedance Z_D; ●, $T_m=46.0$ mK; ▲, $T_m=27.2$ mK; (c) impedance Z_S; ○, $T_m=46.0$ mK; ▲ and ●, $T_m=27.4$ mK; (d) impedance Z_U; $T_m=46.0$ mK.

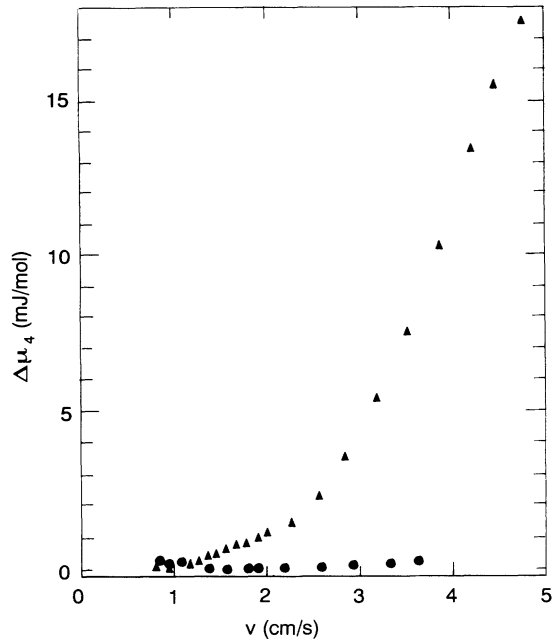

FIG. 8. The $(\Delta\mu_4)$-v dependence measurement with flow impedance Z_K both with (●) and without (▲) superleak shunt.

V. TIME-DEPENDENT EFFECTS

A. Introduction

Two kinds of time-dependent effects were investigated: transient effects, which were observed when the still-heating power $\dot{Q}_s$ was changed, and fluctuations in the pressure difference across a flow impedance during a steady flow of ^{3}He. The time constants of the thermometers, vibrating-wire viscometer, concentration capacitor, and the flow meter were mainly determined by the time constant of the dilution refrigerator as a whole, which was too long for fluctuation measurements. On the other hand, the pressure transducer was able to follow fluctuations with frequencies up to at least 50 Hz. Therefore, the fluctuations and relaxation phenomena were investigated mainly with the pressure transducer.

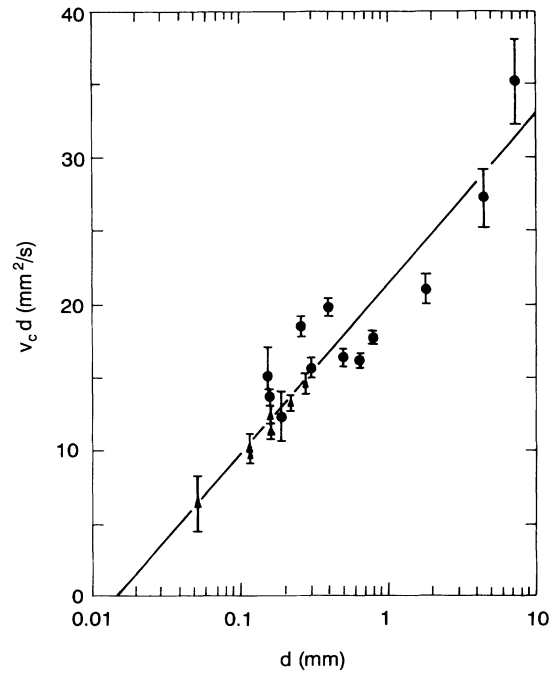

FIG. 9. The product $v_c d$ as a function of the diameter d in a semilogarithmic plot. See also Table I; ●, metal tubes; ▲ , glass tubes. For the capillaries with diameters 0.011 and 0.016 cm the two triangles correspond with v_c and v_{c2}, respectively.

B. Transient effects

If no critical velocities are exceeded μ_4 in the dilute side of the heat exchangers of the dilution refrigerator is constant in the steady state. When $\dot{Q}_s$ is increased stepwise the temperature of the still will rise and some extra ^{3}He will be extracted from the liquid in the still. As a result, μ_4 of the still liquid increases. For a short period of time it will be larger than μ_4 in the mixing chamber. Therefore the superfluid ^{4}He is accelerated through the dilute side of the heat exchangers toward the mixing chamber. There it increases the pressure, and so the ^{3}He flow rate increases. The experiments to be discussed below show that this transient behavior is different for velocities below and above the critical velocity.

The experiment was carried out with a setup where the connection between the mixing chamber and the experimental space (usually Z_m, see Fig. 1) consisted of two flow channels in parallel. One was flow impedance Z_D and the other was a single capillary with the same length and diameter as the capillaries in Z_D (see Table I). One vibrating-wire viscometer was placed downstream of Z_D and one downstream of the single capillary.

A square-wave oscillating heating power $\dot{Q}_s$ was applied to the still with an amplitude of a few percent of the average level. The period was about 2000 s, which is long enough to complete the relaxation process. On a recorder a relatively fast response of the signals in about 100–200 s was observed, followed by a much slower relaxation of about 1000 s. The latter is due to the overall relaxation of the dilution refrigerator. The relaxation time τ, defined as the time after which a signal changed by 50% of the total change, increases sharply at the critical velocity (Fig. 11). The transient behavior is described in detail in Ref. 22.

C. Pressure fluctuations

In this section we will discuss pressure fluctuations which are associated with the critical velocities discussed above. One should be aware that there can be various sources for pressure fluctuations (originating from other parts of the dilution refrigerator) which have nothing to do with critical phenomena in the flow impedance. In general, the fluctuating parameters of the dilution refrigerator as a whole depend on the molar flow rate $\dot{n}$, while the fluctuations due to the critical phenomena in the flow impedances depend on the velocity v. By comparing the results of experiments of impedances which are identical

except for the number of channels in parallel (N), the two sources of fluctuations can be distinguished. Another way to identify external sources of fluctuations is shunting a superleak in parallel with the impedance. When the fluctuations are due to phenomena associated with the critical velocity, they should be absent when the superleak is present.

It was observed that the amplitude of the pressure fluctuations changed strongly around the critical velocity. An example of a recorder trace of the pressure signal when the flow is increased slowly is presented in Fig. 12. At low ^{3}He velocities the fluctuations are small and increase with the velocity. Just below v_c they are large. At v_c their magnitude changes abruptly, becoming very small just above v_c. This effect was seen in many experiments with different flow impedances.

We have the impression that the interesting frequency range lies between 0.5 and 5 Hz. Above 5 Hz no striking features showed up in the spectra. We determined the spectral behavior of the fluctuations of the pressure signal of flow channels Z_K and Z_U. Figure 13 represents the spectrum obtained with impedance Z_K at a velocity of 1.06 cm/s, just below v_c. Peaks are observed which are about 20–40 times higher than the level of the spectra at low velocities. For velocities just above v_c, the peaks are absent. When the velocity is about equal to the second critical velocity v_{c2} (corresponding with the kink in the curve of Fig. 8), two peaks around 0.8 and 1.75 Hz show up. In Fig. 14 the amplitude of the spectrum at 0.85 Hz is shown as a function of v. There are peaks at the critical velocities reflecting the behavior of the velocity dependence of the whole spectrum as discussed above. The behavior shown in Fig. 14 is characteristic for different temperatures and different flow impedances.

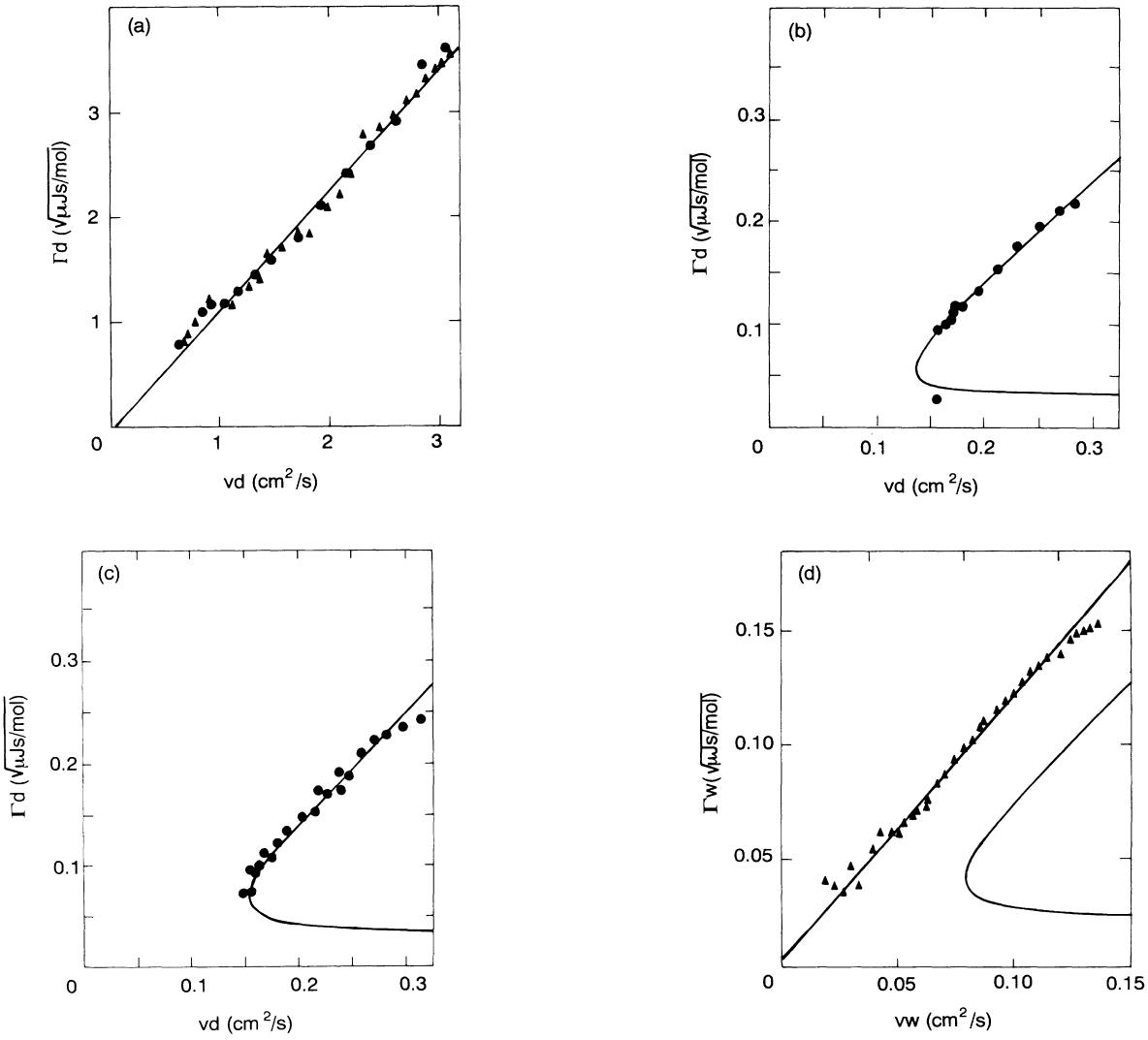

FIG. 10. Fit to the data in terms of the Vinen model [Eqs. (25)–(27)]. (a) Impedance Z_I; ●, $T_m = 56.0$ mK; ▲, $T_m = 37.1$ mK; from the line the value of α is obtained using Eq. (27); (b) impedance Z_D; $T_m = 46.0$ mK; the curve represents a fit to Eq. (25); (c) impedance Z_S; $T_m = 46.0$ mK; the curve represents a fit to Eq. (25); (d) impedance Z_U; $T_m = 46.0$ mK; from the line the value of α is obtained with Eq. (27). The curve is calculated with Eq. (26), using the parameters determined with circular channels.

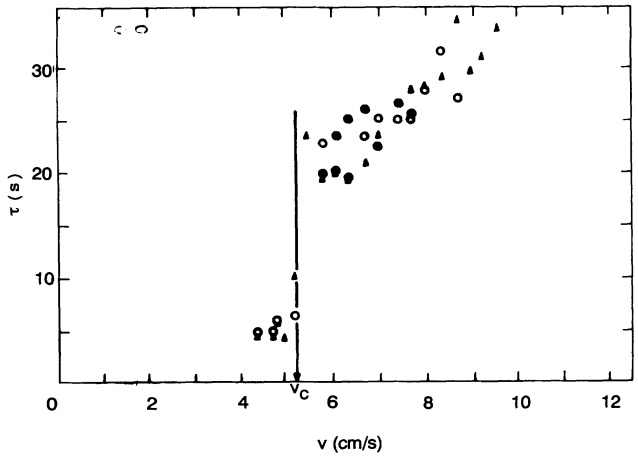

FIG. 11. Relaxation time τ as a function of v. At $v=v_c$ the value of τ changes abruptly (○ and ●, vibrating wires; ▲, pressure cell).

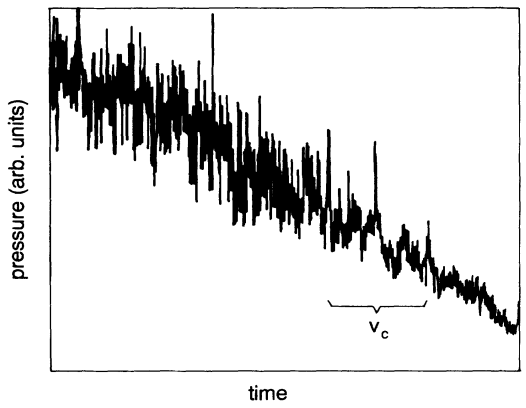

FIG. 12. Typical example (impedance Z_B) of a recorder trace showing the pressure signal as a function of time while the flow is steadily increased. At the critical velocity (indicated) the amplitude of the fluctuations decreases drastically.

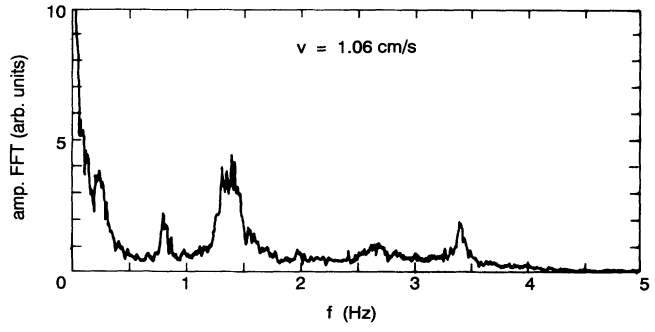

FIG. 13. Fourier spectrum of the pressure fluctuations (in arbitrary units) as obtained for flow impedance Z_K (compare Figs. 8 and 14) without a superleak at a ^{3}He velocity just below the critical value where the amplitude is large. The results are smoothed by averaging every measurement with the two neighboring points on both sides. The sampling time and time constant of the lock-in amplifier both were equal to 100 ms.

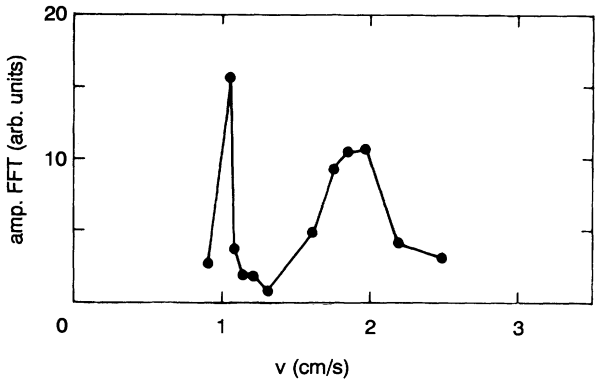

FIG. 14. Amplitude of the pressure fluctuations at 0.85 Hz as function of the velocity v (no superleak parallel). The peaks coincide with the kinks in the $(\Delta\mu_4)$-v dependence represented in Fig. 8.

When a superleak is placed parallel to the flow impedance, the Fourier spectrum does not show any significant structure. The amplitude of the fluctuations is much lower than without the superleak.

The spectra measured with the annular flow channel (Z_U) also show peaks, but these are smaller and do not coincide with the apparent critical velocity. The structure in the spectrum in this case seems to be $\dot{n}$ rather than v dependent,[22] so it is due to fluctuations in the dilution refrigerator rather than in the flow channel.

VI. DISCUSSION

A. Flow properties of mixtures

The flow properties of circular capillaries are in agreement with the mechanical-vacuum model for $v<v_c$. In metal tubes the downstream intrinsic liquid parameters change discontinuously at v_c. The $v_c d$ products corresponding with the minimum values of $v_c d$ of the calculated curves are smaller than the values corresponding with the measured values at the critical velocities. In principle there can be several reasons for this. The first is that at velocities just around v_c there are only a few vortex lines in a tube, and a statistical model like the Vinen model may not be correct in this flow regime. The second reason could be that around v_c the solutions of the steady-state equations are fairly unstable, and v_c can be affected by vortex pinning or by small external influences.

The experimental curves show the same qualitative form as the numerical simulations by Schwarz.[24] From a dimensional analysis of the equation of motion for the vortices[24–27] in pure ^{4}He it follows that

$$v_c d = c_v \frac{\kappa}{4\pi} \ln\left[\frac{c' d}{a_0}\right], \tag{33}$$

where c_v and c' are dimensionless constants. The value

of $c'd$ is of the order of the characteristic radius of curvature of the vortex tangle near onset. Typically c' is in the 0.1–1 range.[27] In Eq. (33), a_0 is the effective core radius, which is on the order of 1 Å in pure ^{4}He. When ^{3}He is trapped in the vortex core,[28–31] the core radius can be relatively large ($\gg 10$ Å for saturated mixtures).[32] However, it is hard to imagine that the core diameter is as large as 1 μm or larger. More experiments, e.g., with small-diameter capillaries, are required to draw definite conclusions.

In glass capillaries the transition at v_c is more gradual. The diameters of the capillaries forming the glass flow impedances vary a few percent. We like to point out that the transition at the critical velocity is a property of the flow impedance as a whole and will be sharp even in the case of a certain distribution of diameters in a bundle of capillaries. It is estimated that the variation of the diameter along a glass tube (in the direction of the flow) is of the same order of magnitude as the variation of the diameter between individual capillaries (less than 3%). A variation of the diameter in the flow direction may lead to a gradual transition in the critical velocity region. Furthermore, the difference in behavior at the critical velocity between metal and glass capillaries is probably due to different pinning properties at the surface.

The critical velocity in annular tubes seems to be below our detection limit. Annular channels follow the mechanical-vacuum model at small velocities because the effect of mutual friction is small. The value of the ^{3}He velocity where the measurements deviate from the mechanical-vacuum model results in an apparent critical velocity v_{ca}, which depends on the measuring accuracy. At high velocities $\Delta\mu_4$ is the same as the high-velocity limit in a circular flow channels. This is an indication that T III (a flow state defined by Tough[10] for slits) is the same as T II for circular flow channels.

The (Γw)-(vw) dependencies calculated for annular flow channels, using the constants α and m obtained from the data of circular capillaries, disagree with the data. This means that our experimental results cannot be explained consistently in terms of the Vinen model.

In all channels the flow state is dominated by mutual friction at very high velocities. In this limit the results confirm the phenomenological expressions found by Castelijns *et al.*[3]

The nonzero $\Delta\mu_4$ values above v_c are attributed to quantum vortices in the flow impedance. The Fourier spectrum of the pressure fluctuations for a fixed frequency as a function of v shows peaks at v_c and at v_{c2}. It is possible that in the critical-velocity region vortices develop in the form of plugs which are unstable and decay again.[33–35]

The spectral technique is possibly a powerful expedient to detect the critical velocity and might be used to analyze the vortex dynamics in the flow of mixtures. Temperature and concentration fluctuations have not been seen up to now and are a challenge for the future.

There are several indications for the existence of a second critical velocity. First of all the flow dependence of the downstream parameters shows a kink at a velocity about twice the first critical velocity. Also, in the cases where a kink is absent, the velocity dependencies at velocities just above the critical velocity do not seem to extrapolate to the high flow-rate values. Furthermore, the amplitude of the pressure fluctuations, plotted as a function of the velocity, shows two peaks.

The detailed velocity dependence of the flow properties in the critical-velocity region is complicated. There are several influences determining the critical velocity. The presence and the magnitude of the second critical velocity is still rather uncertain. Therefore we have no phenomenological relations equivalent to Eqs. (6)–(10) or (11)–(15) describing the flow properties in the critical-velocity region.

B. Comparison with ^{4}He

The flow properties of mixtures have many features in common with the flow properties of pure ^{4}He II.[10,11] E.g., if the parameter B is assumed to be equal to 1, we get $\sqrt{L} = 50$–200 mm^{-1} at velocities just above v_c, which is of the same order of magnitude as in pure ^{4}He II. The values of the critical velocities are also in the same order of magnitude.

In slits in pure ^{4}He thermal counterflow experiments a turbulent flow state, classified by Tough[10] as T III, is observed. In the experiments by Ladner and Tough[36] the transition from laminar flow to T III is shown to be more gradual than in circular capillaries. The transition observed in our experiments with mixtures is also gradual. The values of v_{ca} are of the same order as the values in pure ^{4}He II. In a recent paper, Oestereich and Xie[37] reported results of experiments on He II flow in a narrow slit. In thermal counterflow they found that there was always some vorticity present at least along a part of the channel.

However, there are differences. In general, the distinction between different turbulent states,[10] T I and T II, is in mixtures less pronounced than in pure ^{4}He. In glass tubes we observed a gradual transition at v_c, followed by a steeper transition at a higher velocity (v_{cs}). In the metal tubes at v_c, the transition was sharp and discontinuous most of the time. In metal capillaries usually only one critical velocity without hysteresis was observed in our experiments. The values of the critical velocities in mixtures are a little lower than the values of v_{c2} observed in ^{4}He II counterflow.

Williams and Packard [38] showed that the addition of 5% ^{3}He led to a strong damping of the vortex motion. In general,[39–44] the critical velocity for the formation of vortices by ions does not seem to be influenced very much by the presence of ^{3}He. An important fundamental difference between vortices in mixtures and vortices in pure ^{4}He may be that vortices in mixtures have a nonzero mass. Furthermore, the interaction of individual ^{3}He quasiparticles with vortices may be different from the interaction of ^{4}He excitations as the ^{3}He quasiparticles are fermions. For the same reason one could expect a strong temperature dependence of the flow properties as the temperature in our experiments varies from about 0.05 to 0.25 times the Fermi temperature. Apparently the microscopic quasiparticle-vortex interaction does not play

an important role in the determination of the macroscopic flow properties.

C. Suggestions for further research

It would be of interest to investigate the question of the existence of a critical velocity in slits and annular flow channels. Technically this will be difficult as very long tubes will be necessary. Furthermore, one would like to know the flow properties in capillaries with 10–100-μm diameter to see how the $v_c d$ product extrapolates to low d values. Again it may be difficult to construct a reliable flow impedance of this kind as many short capillaries have to be placed in parallel [Eqs. (30) and (31)]. A dilution refrigerator with small flow rate may be helpful.

In the fluctuation experiments it is of interest to measure locally inside the tubes to check whether turbulent plugs are indeed formed in the flow channel.

The damping constants of second sound due to ^{4}He vortices, which are known for ^{4}He II, are not known for dilute mixtures at low temperature. It is important to measure these parameters using, e.g., second sound. In addition, with second-sound absorption one can probably determine critical velocities for large-diameter tubes ($d > 0.5$ cm), which is impossible with the methods used in this work.

The validity of the Vinen model should be reconsidered. Numerical simulation of the evolution of a vortex tangle[24,25] may be a more appropriate tool to explain the difference in behavior of annular and circular flow channels. Also, pinning mechanisms and the effect of the nonzero mass of the quantum vortices in mixtures on the vortex dynamics should be investigated with numerical simulations.

ACKNOWLEDGMENTS

We would like to thank Professor J. A. Geurst and Dr. J. G. M. Kuerten for their stimulating interest in our work. We owe special thanks to R. Sanders, who has contributed to the data acquisition and analysis. The start of this investigation was strongly stimulated by a discussion between Professor W. J. M. de Jonge and Dr. C. A. M. Castelijns. This work was partly supported by the Dutch Foundation for the Fundamental Research on Matter (FOM), which is financially supported by the Dutch Organization for the Advancement of Research.

[1] I. M. Khalatnikov, *An Introduction to the Theory of Superfluidity* (Benjamin, New York, 1965; reissued Addison-Wesley, New York, 1989).

[2] J. C. Wheatley, R. E. Rapp, and R. T. Johnson, J. Low Temp. Phys. **4**, 1 (1971).

[3] C. A. M. Castelijns, J. G. M. Kuerten, A. T. A. M. de Waele, and H. M. Gijsman, Phys. Rev. B **32**, 2870 (1985).

[4] W. F. Vinen, Proc. R. Soc. London, Ser. A **240**, 114 (1957); **240**, 128 (1957); **242**, 493 (1957); **243**, 400 (1957).

[5] J. Zeegers, J. G. M. Kuerten, A. T. A. M. de Waele, and H. M. Gijsman, in *Proceedings of the 18th International Conference on Low Temperature Physics, Kyoto, 1987,* edited by Y. Nagaoka [Jpn. J. Appl. Phys. **26**, 63 (1987)].

[6] J. Zeegers, R. G. K. M. Aarts, A. T. A. M. de Waele, M. H. W. Verbruggen, and H. M. Gijsman, in *Proceedings of the International Conference on Macroscopic Quantum Phenomena, Smolenice, Czechoslovakia, 1989,* edited by M. Koláč, L. Skrbek, S. Šafrata, and J. Šebek (Smolenice Castle, Czechoslovakia, 1989), p. 228.

[7] J. C. H. Zeegers, A. T. A. M. de Waele, and H. M. Gijsman, J. Low Temp. Phys. **84**, 37 (1991).

[8] R. F. Mudde and H. van Beelen, in *Proceedings of the 18th International Conference on Low Temperature Physics, Kyoto, 1987,* edited by Y. Nagaoka [Jpn. J. Appl. Phys. **26**, 103 (1987)]; Physica B **162**, 197 (1990).

[9] T. Satoh, T. Satoh, T. Ohtsuka, and M. Okuyama, Physica B **146**, 379 (1987); M. Okuyama, T. Satoh, and T. Satoh, *ibid.* **154**, 116 (1988).

[10] J. T. Tough, in *Progress in Low Temperature Physics VIII,* edited by D. F. Brewer (North-Holland, Amsterdam, 1982), p. 133, and references therein.

[11] R. J. Donnelly and C. E. Swanson, J. Fluid Mech. **173**, 387 (1986).

[12] A. T. A. M. de Waele and J. G. M. Kuerten, in *Progress in Low Temperature Physics XIII,* edited by D. F. Brewer (North-Holland, Amsterdam, 1991), and references therein.

[13] J. G. M. Kuerten, C. A. M. Castelijns, A. T. A. M. de Waele, and H. M. Gijsman, Cryogenics **25**, 419 (1985).

[14] C. Ebner and D. O. Edwards, Phys. Rep. **2**, 77 (1971).

[15] H. E. Hall and W. F. Vinen, Proc. R. Soc. London, Ser. A **238**, 204 (1957); **238**, 215 (1957).

[16] R. P. Hudson, H. Marshak, R. J. Soulen, and D. B. Utton, J. Low Temp. Phys. **20**, 1 (1975), especially Chap. 8.

[17] A. C. Anderson, in *Carbon Resistance Thermometry. Temperature, its Measurement and Control in Science and Industry,* edited by H. H. Plumb (Instrument Society of America, Pittsburgh, Pennsylvania, 1972), Vol. 4, Pt. 2, p. 773.

[18] J. F. Schooley, R. J. Soulen, and G. A. Evans, Natl. Bur. Stand. Special Publication **260-44** (U.S. Dept. of Commerce, Washington, DC, 1972).

[19] R. J. Soulen and R. B. Dove, Natl. Bur. Stand. Special Publication **260-62** (U.S. Dept. of Commerce, Washington, DC, 1979).

[20] H. A. Kierstead, J. Low Temp. Phys. **24**, 497 (1976).

[21] B. M. Abraham, O. G. Brandt, G. Eckstein, and J. Manarin, Phys. Rev. **188**, 309 (1969).

[22] J. Zeegers, Ph.D. thesis, Eindhoven University of Technology, 1991 (unpublished).

[23] J. F. Allen and J. Reekie, Proc. Cambridge Philos. Soc. **35**, 114 (1939).

[24] K. W. Schwarz, Phys. Rev. Lett. **50**, 364 (1983).

[25] K. W. Schwarz, Phys. Rev. B **38**, 2398 (1988).

[26] C. E. Swanson, Ph.D. thesis, Oregon University, 1985 (unpublished).

[27] C. E. Swanson and R. J. Donnelly, J. Low Temp. Phys. **61**, 363 (1985).

[28] G. W. Rayfield and F. Reif, Phys. Rev. **136**, A1194 (1964).

[29] T. Ohmi, T. Tsuneto, and T. Usui, Prog. Theor. Phys. **41**, 1395 (1969).

[30] L. S. Rent and I. Z. Fisher, Zh. Eksp. Teor. Fiz. **55**, 722 (1968) [Sov. Phys. JETP **28**, 375 (1969)].

[31] L. Senbetu, J. Low Temp. Phys. **32**, 571 (1978).

[32]T. Ohmi and T. Usui, Prog. Theory. Phys. **41**, 1401 (1969).
[33]D. Griswold, C. P. Lorenson, and J. T. Tough, Phys. Rev. B **35**, 3149 (1987); D. Griswold and J. T. Tough, Phys. Rev. A **36**, 1360 (1987).
[34]G. Marees and H. van Beelen, Physica B **145**, 21 (1987).
[35]R. P. Slegtenhorst, G. Marees, and H. van Beelen, Physica B+C **113B**, 367 (1982).
[36]D. R. Ladner and J. T. Tough, Phys. Rev. B **17**, 1455 (1978).
[37]T. Oestereich and J. K. Xie, J. Low Temp. Phys. **83**, 57 (1991).
[38]G. A. Williams and R. E. Packard, Phys. Rev. Lett. **33**, 280 (1974).
[39]C. M. Muirhead, W. F. Vinen, and R. J. Donnelly, Philos. Trans. R. Soc. London, Ser. A **311**, 433 (1984).
[40]C. M. Muirhead, W. F. Vinen, and R. J. Donnelly, Proc. R. Soc. London, Ser. A **402**, 225 (1985).
[41]R. M. Bowley, J. Phys. C **17**, 595 (1984).
[42]R. M. Bowley, G. G. Nancolas, and P. V. E. McClintock, Phys. Rev. Lett. **52**, 659 (1984).
[43]E. Varoquaux, M. W. Meisel, and O. Avenel, Phys. Rev. Lett. **57**, 2291 (1986).
[44]G. G. Nancolas, R. M. Bowley, and P. V. E. McClintock, Philos. Trans. R. Soc. London, Ser. A **313**, 537 (1985).